ETMM13: The 13th International ERCOFTAC symposium on engineering, turbulence, modelling
Rhodes, Greece, 15-17 September, 2021

Detached Eddy Simulation coupled with steady RANS in the wall region

Lars Davidson

Division of Fluid Dynamics, Department of Mechanics and Maritime Sciences
Chalmers University of Technology, SE-412 96 Gothenburg, Sweden
lada@chalmers.se

Abstract

Xiao & Jenny (2012) proposed an interesting hybrid LES/RANS method in which they use two solvers and solve the RANS and LES equations in the entire computational domain. In the present work this method is simplified and used as a hybrid RANS-LES method, a *wall-modeled* LES. The two solvers are employed in the entire domain. Near the walls, the flow is governed by the steady RANS solver; drift terms are added to the DES equations to ensure that the time-integrated DES fields agree with the steady RANS field. Away from the walls, the flow is governed by the DES solver; in this region, the RANS field is set to the time-integrated LES field. The disadvantage of traditional DES models is that the RANS models in the near-wall region – which originally were developed and tuned for steady RANS – are used as URANS models where a large part of the turbulence is resolved. In the present method – where steady RANS is used in the near-wall region – the RANS turbulence models are used in a context for which they were developed. In this method, it may be worth while to use an accurate, advanced RANS model. The EARSM model is used in the steady RANS solver. The new method is called **NZ S-DES** . It is found to substantially improve the predicting capability of the standard DES. A great advantage of the new model is that it is insensitive to the location of the RANS-LES interface.

1 Introduction

DES (Detached-Eddy Simulation) uses unsteady RANS near walls (URANS region) and LES further away from walls (LES region). The resolved turbulence in the URANS region is often larger than the modeled part. But the RANS models used in the URANS region were originally developed and tuned in steady RANS simulations. Hence the accuracy and the validity of the RANS models in the URANS region can be questioned. In the present work, DES is coupled with *steady* RANS near the walls. We denote the method NZ S-DES (Non-Zonal approach using Steady RANS coupled to DES).

Xiao & Jenny (2012), Xiao et al. (2013) proposed a new method in which they solve both the LES and RANS equations in the entire domain. The flow is in the near-wall region governed by the RANS equations and in the outer region it is governed by the LES equations. This is achieved by adding drift terms in the LES and RANS equations. In the interface region(s), the drift terms are modified by a linear ramp function. Drift terms are used in all equations in the RANS equations (momentum equations, the pressure equation (PISO is used)) and in the modelled turbulent equations (k and ε). Two drift terms are added in the LES momentum equations; one to ensure than the mean velocity fields in the RANS and LES equations are the same and one to ensure that the total turbulent kinetic energies are the same.

In the present study, the steady RANS equations are solved. Here it makes sense to use advanced RANS turbulence models, since these models were developed for steady RANS. The EARSM (Wallin & Johansson 2000) is used in the RANS solver. The present method is in many aspects similar to that proposed by Xiao & Jenny (2012), Tunstall et al. (2017) but it is simplified: the RANS equations are used in steady mode, a more advanced RANS turbulence model is used and the present method includes fewer drift terms and tuning constants.

2 Numerical solvers

The momentum equations with an added turbulent viscosity read

$$\frac{\partial \bar{v}_i}{\partial t} + \frac{\partial \bar{v}_j \bar{v}_i}{\partial x_j} = \delta_{1i} - \frac{1}{\rho}\frac{\partial \bar{p}}{\partial x_i} + \frac{\partial}{\partial x_j}\left((\nu + \nu_t)\frac{\partial \bar{v}_i}{\partial x_j} \right) \quad (1)$$

where the first term on the right side is the driving pressure gradient in the streamwise direction, which is used in the fully-developed channel flow simulations.

DES solver

An incompressible, finite volume code is used. The convective terms in the momentum equations

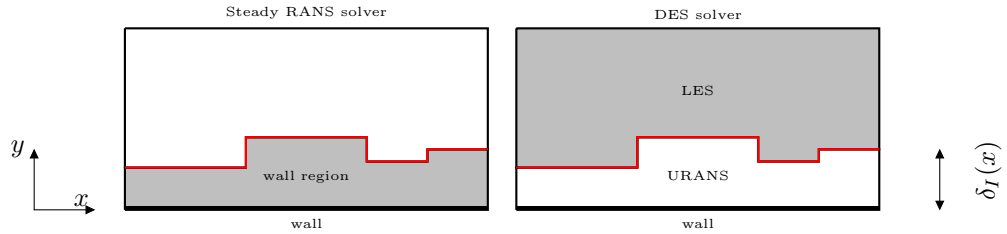

(a) Steady RANS solver (b) DES solver

Figure 1: Grey color indicates the solver that drives the flow. The interface, I, is shown in red.

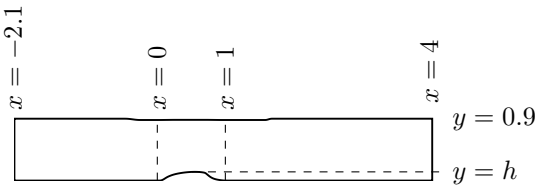

Figure 2: The domain of the hump. $z_{max} = 0.3$.

are discretized using central differencing. Hybrid central/upwind is used for the k and ω equations. The Crank-Nicolson scheme is used for time discretization of all equations. The numerical procedure is based on an implicit, fractional step technique with a multigrid pressure Poisson solver and a non-staggered grid arrangement.

RANS solver

An incompressible, finite volume code – CALC-BFC – is used. The transient term in Eq. 1 (the first term on the left side) is not included. The convective terms in the momentum equations are discretized using the second-order bounded scheme, MUSCL (van Leer 1979). Hybrid central/upwind is used for the k and ω equations. The numerical procedure is based on pressure-correction method, SIMPLEC, and a staggered grid arrangement.

3 The NZ S-DES method

Two sets of equations are solved (steady RANS solver, see Fig. 1(a) and DES solver, see Fig. 1(b)) in the entire domain on identical grids. The steady RANS solver may be two dimensional (as in the present work). Drift terms are added in the DES equations, S_i^{DES}, in the wall region, see Fig. 1(a). The drift terms in the DES velocity equations read

$$S_i^{DES} = \frac{\langle v_i^{RANS}\rangle_T - \langle \bar{v}_i^{DES}\rangle_T}{\tau_r} \qquad (2)$$

where $\tau_r = \max(0.1k/\varepsilon, \Delta t)$ following Tunstall et al. (2017). No drift term is used in the pressure equation. $\langle\cdot\rangle_T$ indicates integration over time, T, i.e.

$$\begin{aligned} \langle\phi(t)\rangle_T &= \frac{1}{T}\int_{-\infty}^{t}\phi(\tau)\exp(-(t-\tau)/T)d\tau \Rightarrow \\ \langle\phi\rangle_T^{n+1} &\equiv \langle\phi\rangle_T = a\langle\phi\rangle_T^n + (1-a)\phi^n, \end{aligned} \qquad (3)$$

where $a = 1/(1+\Delta t/T)$ and n denotes the timestep number. Note that although the flow cases in the present work include homogeneous direction(s), no space averaging is made in Eq. 3. It may be noted that although the velocity field in the RANS solver is steady, it is time integrated when used in Eqs. 2 and 4 because it varies slightly in time. This time integration is probably not necessary.

In the LES region, the RANS velocities are prescribed as $v_i^{RANS} = \langle v_i^{LES}\rangle_T$ by adding a large source term, i.e.

$$S_i^{RANS} = \frac{\langle v_i^{LES}\rangle_T - \langle \bar{v}_i^{RANS}\rangle_T}{\epsilon} \qquad (4)$$

where $\epsilon = 10^{-10}$. The pressure is simply set as $\bar{p}^{RANS} = \langle p^{LES}\rangle_T$ and the pressure correction is set to zero. This means that, in reality, the steady RANS solver needs to be solved only in the wall region. In the LES region, the momentum equations in the RANS solver are merely transporting the turbulence quantities, k and ω, to ensure that correct values of k and ω are transported into the RANS region through the RANS-LES interface at $y = \delta_I$, see Fig. 1. The pressure, $\langle \bar{p}_{j+1}^{LES}\rangle_T$, and the streamwise velocity, $\langle \bar{v}_{j+1}^{LES}\rangle_T$, at the RANS-LES interface are used as a boundary condition for the RANS equations in the wall region, see Fig. 3. The wall-normal velocity, $\bar{v}_j^{RANS}$, is solved for using the pressure at node $j+1$. The RANS solver is called every 10th time step.

The $k-\omega$ DES model

The Wilcox $k-\omega$ turbulence DES model reads

$$\begin{aligned} \frac{dk}{dt} &= P^k + \frac{\partial}{\partial x_j}\left[\left(\nu + \frac{\nu_t}{\sigma_k}\right)\frac{\partial k}{\partial x_j}\right] - F_{DES}C_\mu k\omega \\ \frac{d\omega}{dt} &= C_{\omega_1}\frac{\omega}{k}P^k - C_{\omega 2}\omega^2 + \frac{\partial}{\partial x_j}\left[\left(\nu + \frac{\nu_t}{\sigma_\omega}\right)\frac{\partial \omega}{\partial x_j}\right] \\ \nu_t &= \frac{k}{\omega} \end{aligned} \qquad (5)$$

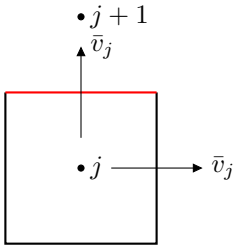

Figure 3: Control volume, j, in the wall region (RANS solver) adjacent to the interface, I (in red).

where $d/dt = \partial/\partial t + \bar{v}_j \partial/\partial x_j$ ($\partial/\partial t = 0$ in the RANS solver). The standard coefficients are used, i.e. $C_{\omega 1} = 5/9$, $C_{\omega 2} = 3/40$, $\sigma_k = \sigma_\omega = 2$ and $C_\mu = 0.09$. The F_{DES} function is computed as

$$F_{DES} = \max\left\{\frac{L_t}{\Delta}\right\} = \max\left\{\frac{k^{1/2}/(C_\mu \omega)}{\Delta}\right\} \quad (6)$$

The LES length scale, Δ, is used from DES (Spalart et al. 1997), i.e.

$$\Delta = C_{DES}\Delta_{max}, \quad \Delta_{max} = \max\{\Delta x, \Delta y, \Delta z\} \quad (7)$$

The DES equations are solved in the entire region, but they govern the flow only in the LES region, see Fig. 1. The location of the interface *in* the DES solver is defined in the same way as *between* the RANS solver and the DES solver, i.e. where $F_{DES} = 1$, see Eq. 6.

The $k-\omega$ EARSM model in the RANS solver

The steady RANS equations are solved in the entire region, but they govern the flow only in the RANS region, see Fig. 1. The $k-\omega$ in Eq. 5 is used with $F_{DES} = 1$ and the transient terms are set to zero. The Reynolds stresses, $\overline{v_i' v_j'}$, are computed from the two-dimensional explicit algebraic Reynolds stress model (EARSM) (Wallin & Johansson 2000).

Initialization

The simulations are initialized as follows: first the 2D RANS equations are solved. Anisotropic synthetic fluctuations, $(\mathcal{V}_i')_m$, are then superimposed to the 2D RANS field which gives the initial LES velocity field. The initial time integrated fields, $\langle v_i^{LES}\rangle_T$ and $\langle v_i^{RANS}\rangle_T$, are also set from the 2D RANS field.

In order to compute $(\mathcal{V}_i')_m$, synthetic fluctuations, $v_{i,synt}'$, are computed plane-by-plane $(y-z)$ in the same way as prescribing inlet boundary conditions. The synthetic fluctuations in the $y-z$ planes are coupled with an asymmetric space filter

$$(\mathcal{V}_i')_m = a(\mathcal{V}_i')_{m-1} + b(v_{synt,i}')_m \quad (8)$$

where m denotes the index of the x_1 location and $a = \exp(-\Delta x_1/L_{int})$ and Δx_1 and L_{int} denote the grid size and the integral length scale, respectively ($L_{int} = 0.2$).

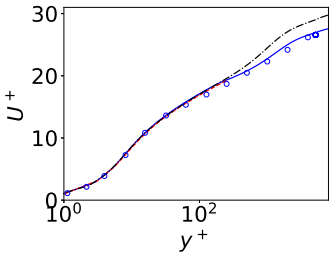

Figure 4: Channel flow. NZ S-DES compared with standard DES. ——: DES solver in NZ S-DES; – –: RANS solver in NZ S-DES; –·–: Standard DES; ○: Reichardt's law, $U^+ = \frac{1}{\kappa}\ln(1-0.4y^+) + 7.8\left[1-\exp(-y^+/11) - (y^+/11)\exp(-y^+/3)\right]$.

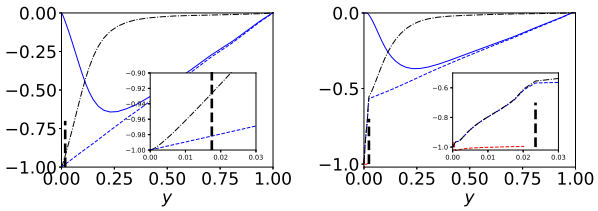

Figure 5: Channel flow. Standard DES (left) and NZ S-DES (right). Shear stresses scaled with u_τ^2. Vertical black dashed lines show predicted RANS-LES interface. ——: resolved; –·–: viscous + modeled; – –: total. – –: viscous plus modeled in RANS solver (EARSM) in NZ S-DES.

4 Results

Fully-developed channel flow

The first test case is fully developed channel flow with periodic boundary conditions in streamwise (x) and spanwise (z) directions. The Reynolds number, $Re_\tau = u_\tau h/\nu$, is 8 000 where h denotes half-channel width. The size of the domain is $x_{max} = 3.2$, $y_{max} = 2$ and $z_{max} = 1.6$. The mesh has $32 \times 96 \times 32$ (x, y, z) cells. $\Delta z^+ = 400$ and $\Delta x^+ = 800$. The timestep is set to $\Delta \hat{t} \equiv \Delta t U_b/h = 0.025$ (U_b denotes bulk velocity) which gives $CFL < 0.4$. In Davidson (2019) the influence of the integration times, T (see Eq. 3), was evaluated. It was found that it is important that the sampling time is much larger than the integration time, T. If it is too small, it often gives an asymmetric time-averaged flow field. Here, the sampling time, $\mathcal{T}$, to reach fully developed condition and sampling time are both set to $\hat{\mathcal{T}} \equiv \mathcal{T} U_b/h = 1000$. The integration time is set to $\hat{T} \equiv T U_b/h = 1$. Values of up to $\hat{T} = 50$ were evaluated in Davidson (2019) with negligible influence on the results.

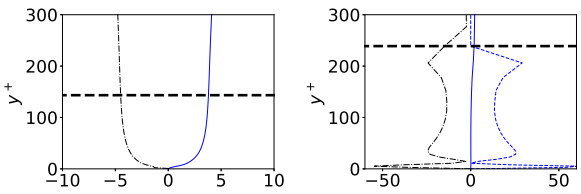

Figure 6: Channel flow. Standard DES (left) and NZ S-DES (right). Forces in the $\langle \bar{v}_1 \rangle$ equation (normalized with u_τ^2/δ). Thick black dashed line shows the predicted RANS-LES interface. ▬: $-\frac{\partial \langle \langle \bar{u}'\bar{v}' \rangle \rangle}{\partial x_2}$; ▬·▬: $\frac{\partial}{\partial x_2}\left(\langle \nu_{tot} \rangle \frac{\partial \langle \bar{v} \rangle}{\partial x_2} \right)$; ▬▬: Drift term, S_1^{DES}, see Eq. 2.

Figure 4 compares the velocity profiles obtained with NZ S-DES with that of standard DES. The velocity profiles predicted with NZ S-DES agree very well with Reichardt's law whereas the standard DES exhibits the usual log-layer mismatch.

Figure 5 shows the shear stresses. We find that the magnitude of the resolved shear stress is much smaller for NZ S-DES than for standard DES. As a consequence, NZ S-DES also gives a much smaller total shear stress. In fully developed channel flow, the total (resolved, modeled and viscous) shear stress is given by

$$\tau_{tot}^+ = \tau_w^+ \left(1 - \frac{y}{h}\right). \qquad (9)$$

where subscript denotes scaling with u_τ^2. Normally, $\tau_w^+ = 1$ because the driving pressure gradient is equal to one (the first term on the right side of Eq. 1). For standard DES (Fig. 5, left figure), the stresses and the driving pressure gradient are in balance and as a result the total shear stress varies linearly as dictated by Eq. 9. However, for NZ S-DES the total shear stress does not exhibit a linear behaviour (Fig. 5, right figure). Xiao et al. (2013) also report that the drift term affects the resolved shear stresses. In NZ S-DES the wall shear stress, τ_w^+, balances not only the driving pressure gradient but also the drift term. As a result, τ_w^+ increases. Figure 6 presents the forces acting in the streamwise momentum equation, i.e. the gradient of the resolved, modelled and viscous shear stresses, the driving pressure gradient – and for NZ S-DES – also the drift term, S_1^{DES}, see Eq. 2. Here we see the effect of the drift term in the DES equations. The drift term drives (increases) – as it should – the time-integrated DES velocity, $\langle \bar{v}_1 \rangle_T$ towards the RANS velocity. The drift term is mainly balanced by the modeled shear stress force (close to the wall it is balanced by the viscous shear stress force). It may be noted that they are very large; the modeled shear stress force

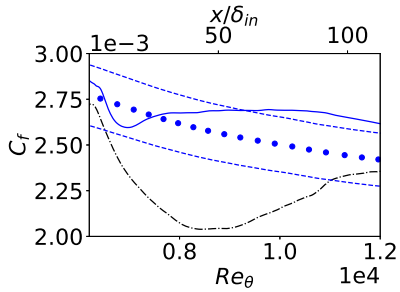

(a) Skinfriction v. momentum thickness. ○: expts; ▬▬: ±6%

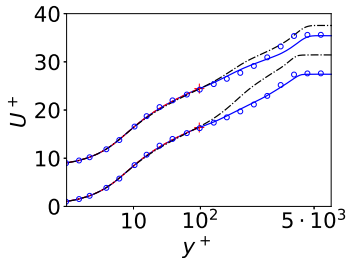

(b) Mean velocity. Lower lines: $x/\delta_{in} = 37$, $Re_\theta = 8\,900$; upper lines: $x/\delta_{in} = 75$,$Re_\theta = 11\,800$

Figure 7: Boundary layer flow. ▬: NZ S-DES; ▬·▬: Standard DES; ▬▬: RANS solver in NZ S-DES.

is much much larger than that using standard DES (see Fig. 6). It should, however, be recalled that the large drift term is active in a thin region close to the walls. The large shear stress force for the NZ S-DES is understood by looking at the viscous plus modeled shear stress in Fig. 5. In the URANS region it changes from its wall value of -1 to approximately $\tau_I^+ = -0.55$. In the LES region, the total shear stress for NZ S-DES balances the pressure gradient but the slope is different from that in Eq. 9 (see Fig. 6). The form reads

$$\tau_{tot}^+ = \tau_I^+ \left(1 - \frac{y - y_I}{h}\right). \qquad (10)$$

where subscript I denotes the URANS-LES interface. It may be pointed out that the drift term has no physical meaning: its object is simply to make the time-integrated DES velocity match the RANS profile, see Eq. 2. Figure 5 also presents viscous plus modeled EARSM shear stress for NZ S-DES in the RANS solver (see inset). As expected, it is much larger than the corresponding term in the DES solver. The location of the interface is furthermore indicated and it can be seen that NZ S-DES puts the interface further away from the wall than the standard DES simulation does (see also Fig. 6).

Flat-plate boundary layer

The second test case is developing boundary

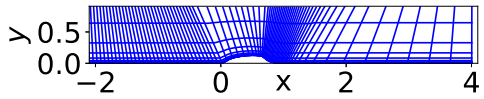

Figure 8: Hump flow. Grid.

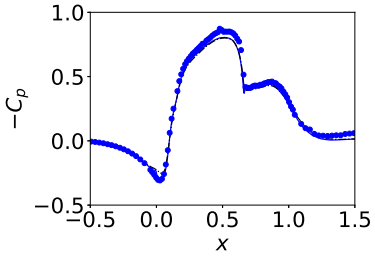

(a) Pressure coefficient.

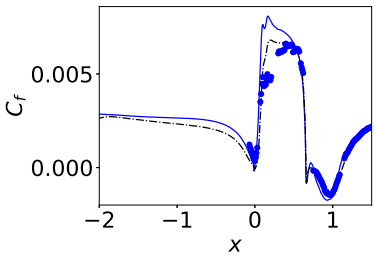

(b) Skinfriction.

Figure 9: Hump flow. ——: NZ S-DES; – · – –: standard DES.

layer along a flat plate. The mean inlet profiles are taken from a 2D RANS solution at $Re_\theta = 6100$. The mesh has $1024 \times 160 \times 64$ cells (x, y, z) with $\Delta t = 0.002$. The far-field mean velocity is one, i.e. $U_{free} = 1$. The spanwise extent of the domain is $z_{max} = 2\delta_{in}$. Twice that, i.e. $2z_{max}$, has been evaluated which confirms that z_{max} is sufficiently large. The length (x) and height (y) of the domain is $21\delta_{in}$ and $112\delta_{in}$, respectively. $\Delta z^+_{in} = 85$ and $\Delta x^+_{in} = 280$. Anisotropic, synthetic turbulence is superimposed to the 2D RANS velocity profiles at the inlet. The procedure is described in Davidson (2016), Arvidson et al. (2018). The inlet turbulent length scale is set to $L_t = 0.3\delta_{in}$.

Figure 7 presents the skin friction and the mean velocities which are both much better predicted with the NZ S-DES model than the standard DES model. It can be noted that the interface is located too close to the wall (at $y^+ \simeq 100$). It was found in Deck et al. (2014) that when the interface is located too close to the wall, the standard DES gives poor results.

Hump flow

The third test case is the flow over a two-dimensional hump, see Fig. 2. The Reynolds number of the hump flow is $Re_c = 936\,000$, based on the hump length, $c = 1$, and the inlet mean velocity at the centerline, $U_{in,c} = 1$. The inlet is located at $x = -2.1$ and the outlet at $x = 4.0$, see Fig. 2. The mesh has $650 \times 110 \times 66$ cells (x, y, z) and it is based on the mesh from the NASA workshop[1] but it is refined upstream of the hump and in the outlet region, see Fig. 8. The spanwise extent of the domain is set to 0.3 so that $\Delta z = z_{max}/nk = 0.3/64 = 0.0047$.

The inlet profiles are taken from a separate 2D RANS simulation with the same momentum thickness as the boundary layer in the experiments (Greenblatt et al. 2004, 2005). Anisotropic synthetic fluctuations are superimposed to the inlet velocity profile in the same way as for the boundary-layer simulations. Periodic boundary conditions are used in the spanwise direction (z). The interface between the URANS and the LES region as well at that between the steady RANS solver and the DES solver is – as in the channel flow and the boundary-layer simulations – defined by Eq. 6.

The pressure coefficient and skin friction are presented in Fig. 9. As can be seen, the agreement with experiments is good for both NZ S-DES and standard DES. The most obvious discrepancy is the large skin friction predicted by NZ S-DES at $x \simeq 0.17$ and that the standard DES predicts slightly too low a skin friction upstream of the hump (as was also seen for the boundary layer flow, Fig. 7(a)). These two discrepancies are probably connected: the under-predicted skin friction by the standard DES gives a smaller velocity on the upstream part of the hump and hence a smaller skin friction than NZ S-DES. Hence, the fact that the skin friction is better predicted than NZ S-DES at $x \simeq 0.17$ is probably fortuitous, due to a poor predicted in-coming boundary layer.

Figure 10 compares the predicted velocity profiles with experiments. The NZ S-DES and standard DES give virtually identical velocity profiles. The NZ S-DES predicts somewhat too strong a backflow (see Fig. 10, $x = 0.80$). The velocity profiles of the RANS solver are also included. The RANS solver velocity profiles in the wall region match those of the DES solver as they should. The locations of the interface is shown with a red plus sign. It may be noted that the location of the interface at $x = 1.3$ is further away from the wall compared to at $x = 0.65, \ldots, x = 1.1$.

5 Conclusions

The paper presents a new non-zonal model based on a steady RANS solver in the wall region coupled with a DES solver which covers the entire region. The steady RANS solver is called very 10th timestep. It could probably be called less frequently. The RANS solver dictates the flow in the wall – i.e. the URANS – region. A drift term in

[1] https://turbmodels.larc.nasa.gov/nasahump_val.html

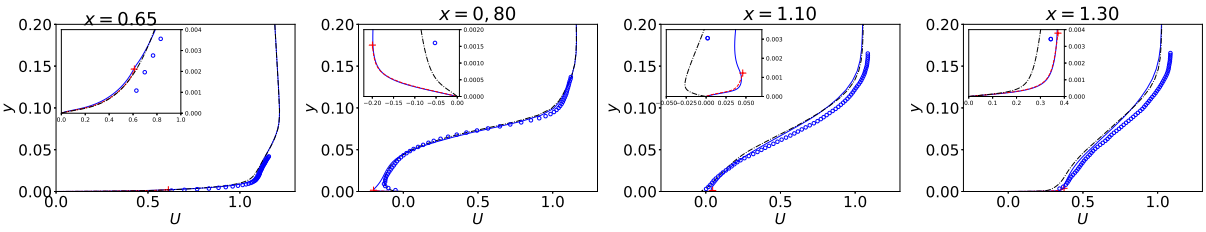

Figure 10: Hump flow. Velocities. +: predicted RANS-LES interface; ▬: NZ S-DES , DES solver; ▬ ▬: NZ S-DES , RANS solver; ▬ · ▬: standard DES; ○: exp; +.

the wall region in the DES solver forces the time-integrated DES flow to match that of the RANS flow. For the channel flow, this term is large as it forces – as it should – the time-averaged LES field to agree with the steady RANS field in the RANS region,

The new model is evaluated in fully developed channel flow, flat-plate boundary layer and the hump flow. The new model gives very good agreement with experiments. It is found to substantially improve the predicting capability of the standard DES. It is found (but not shown due to space limitations) that when the DES length scale in Eq. 7 is replaced by the IDDES length scale, the RANS-LES interface is moved much closer to the wall. But the new model still gives good results which shows that new model is insensitive to the location of the RANS-LES interface which is great advantage. Another advantage is that it make sense to use advanced RANS turbulence models since they in NZ S-DES are used in a context (steady flow) for which they were developed.

The disadvantage is of course the complexity it entails to use two solvers and the additional CPU time. Since the time-averaged flow for all test cases in the present work are two dimensional, a two-dimensional RANS solver was employed and hence the additional CPU time was negligible. In three-dimensional flows, one could consider to use the RANS solver only in the URANS region, and solve the k and ω equations using the time-averaged LES velocities, $\langle \bar{v}_i \rangle_T$, see Eq. 3.

References

Arvidson, S., Davidson, L. & Peng, S.-H. (2018), 'Interface methods for grey-area mitigation in turbulence-resolving hybrid RANS-LES', *Int. J. of Heat and Fluid Flow* **73**, 236–257.

Davidson, L. (2016), 'Zonal PANS: evaluation of different treatments of the RANS-LES interface', *J. of Turb.* **17**(3), 274–307.

Davidson, L. (2019), Non-zonal detached eddy simulation coupled with a steady RANS solver in the wall region, Vol. 120 of *ERCOFTAC Bull.*, pp. 43–48.

Deck, S., Renard, N., Laraufie, R. & Sagaut, P. (2014), 'Zonal detached eddy simulation (ZDES) of a spatially eveloping flat plate turbulent boundary layer over the reynolds number range 3 150 $\leq Re_\theta \leq$ 14 000', *Physics of Fluids A* **26**(025116).

Greenblatt, D., Paschal, K. B., Yao, C.-S. & Harris, J. (2005), 'A separation control CFD validation test case Part 1: Zero efflux oscillatory blowing', AIAA-2005-0485.

Greenblatt, D., Paschal, K. B., Yao, C.-S., Harris, J., Schaeffler, N. W. & Washburn, A. E. (2004), 'A separation control CFD validation test case. Part 1: Baseline & steady suction', AIAA-2004-2220.

Spalart, P. R., Jou, W.-H., Strelets, M. & Allmaras, S. R. (1997), Comments on the feasability of LES for wings and on a hybrid RANS/LES approach, *in* C. Liu & Z. Liu, eds, 'Advances in LES/DNS, First Int. conf. on DNS/LES', Greyden Press, Louisiana Tech University.

Tunstall, R., Laurence, D., Prosser, R. & Skillen, A. (2017), 'Towards a generalised dual-mesh hybrid LES/RANS framework with improved consistency', *Computers & Fluids* **157**, 73–83.

van Leer, B. (1979), 'Towards the ultimate conservative difference scheme. V. A second-order sequel to godonov's method', *J. of Comp. Phys.* **32**, 101–136.

Wallin, S. & Johansson, A. V. (2000), 'A new explicit algebraic Reynolds stress model for incompressible and compressible turbulent flows', *Journal of Fluid Mechanics* **403**, 89–132.

Xiao, H. & Jenny, P. (2012), 'A consistent dual-mesh framework for hybrid LES/RANS modeling', *J. of Comp. Phys.* **231**, 1848–1865.

Xiao, H., Sakai, Y., Henniger, R., Wild, M. & Jenny, P. (2013), 'Coupling of solvers with non-conforming computational domains in a dual-mesh hybrid LES/RANS framework', *Computers & Fluids* **88**, 653–662.